15TH IEA HEAT PUMP CONFERENCE
MAY 26–29, 2026 | HOFBURG
VIENNA 2026
DECARBONISATION THROUGH INNOVATION

Optimized use of ground collector thermal energy storage in a heat pump system with different ambient heat sources

Annemarie Lauffer*, Christian Schweigler

CENERGIE - Center for Energy-Efficient Buildings and Districts, HM Hochschule München University of Applied Sciences, Lothstr. 34, 80335 Munich, Germany

Abstract

The seasonal performance of heat pump systems can be increased by using ground-based heat sources like geothermal wells, horizontal ground collectors, or groundwater wells. For sites with restrictions on ground-based heat sources or limited property areas, a heat pump system with building-integrated heat sources is used to achieve high energy efficiency.
A solar absorber integrated into the façade of a building regenerates a horizontal ground collector thermal energy storage located beneath the building, which serves as a heat source for the heat pump. The ground collector's area is limited by the size of the building's ground floor and therefore used as medium-term storage. To complement the contribution of the two building-integrated heat sources, an ambient air heat exchanger is integrated in the system. A simulation model of the system is used to optimize the use of available ambient heat sources throughout the entire heating season.
Due to its position underneath the building, freezing of the underground heat storage must be avoided. Therefore, a variable-speed heat pump is used to operate with reduced heat extraction, enabling a deeper discharge of the storage while keeping the brine loop outlet temperature above freezing. Control strategy setups for optimal utilization of the heat sources, including a night setback of the heat supply, are developed.
The proportion of the underground heat storage relative to the other ambient heat sources increases from 40 % for a single-speed heat pump to 52 % for a variable-speed heat pump and to 61 % when the night setback is applied. Through the increased utilization, less heat extraction from ambient air is required on cold winter days, resulting in an increase of the seasonal performance from 3.99 to 4.63 and 4.91, respectively.
The heat pump system is compared with an air-source heat pump with a seasonal performance of 4.29.

Keywords: Heat pump systems; medium-term storage; underground heat storage; solar absorber; regeneration

1. Introduction

Electrical heat pumps play an important role for the transformation of the heating sector. As their efficiency rises with higher heat source temperatures, ground-sourced heat pumps are preferable to air-source heat pumps [1]. Contrasting to this, 92 % of the newly installed heat pumps in Germany are air-source heat pumps [2]. This is due to lower investment cost and easier installation compared to ground-source heat pumps. In addition, there are other restricting factors for ground-source heat pumps, like an unsuitable ground structure, local regulations for the use of ground water or deep geothermal wells, or limited size of the ground area, restricting the use of horizontal ground collectors.

In order to overcome these limitations and achieve a high seasonal efficiency, a heat pump system with multiple heat sources is developed. The system comprises three building-integrated heat sources, namely an ambient air heat exchanger "AAHX", a massive solar thermal collector "MSTC", as reviewed in [3-4], and a ground collector thermal energy storage "GCTES". The GCTES is installed underneath the building and is

* Corresponding author. *E-mail address:* annemarie.lauffer@hm.edu

restricted to the size of the ground slab of the building above. Its heat content is further limited by the requirement that the surrounding earth must not be frozen in order to prevent damage to the building's structure. The GCTES offers the highest heat source temperature compared to the other heat sources on cold winter days. However, its heat content is restricted. Therefore, in order to ensure the effective operation of the heat pump system with multiple heat sources, it is necessary to incorporate different aspects into the control strategy. In general, due to its limited heat content, underground heat storage must be withheld for the purpose of utilizing it during the colder winter days. Yet, as long as the storage remains at an elevated temperature, regeneration of the GCTES by solar heat gained by the MSTC is hindered, resulting in a reduced contribution of the underground heat storage relative to the other ambient heat sources on an annual basis. Thus, an operating strategy must be developed for coordinated utilization of all ambient heat sources, aiming at maximum seasonal performance of the heat pump system. For this purpose, a medium-term heat storage management is applied instead of a seasonal approach, aiming at maximum inter-seasonal regeneration allowing for continuous availability of the underground heat storage to avoid air-sourced operation of the heat pump during severe winter conditions.

This paper describes the system concept for the heat pump system, which has been realized in a pilot installation with monitored operation since November 2020. To optimize the control strategy of the system, a simulation model is developed that considers both the individual components validated with measurement data and their interaction within the system. Different options for the control strategy of the system are described. Based on the results of the system model, the question is discussed whether a variable-speed heat pump – as opposed to a single-speed heat pump – as well as a night setback of the heat supply, would facilitate enhanced heat extraction from the underground heat storage. This, in turn, is hypothesized to result in increased inter-seasonal regeneration of the storage and higher seasonal performance of the heating system.

2. System concept

Aiming at a high heat pump system efficiency, an air-source heat pump system is extended by two additional heat sources. The three heat sources are connected to the brine/water heat pump via a brine circuit. The AAHX is constructed like in a regular air-source heat pump but uses brine as a heat transfer fluid instead of direct evaporation of the refrigerant of the heat pump. The MSTC is constituted by the outer shell of a concrete-sandwich prefabricated wall, which is equipped with a PE tube meander to facilitate heat extraction by the brine loop, as described in [5]. It comprises three wall modules with an overall surface area of 37,8 m². The façade elements are not glazed and therefore reach only medium-high temperatures, which allows for the integration in a heat pump system. The MSTC is well suited for architectural integration, as the façade integrated collector cannot be differentiated from the other wall surfaces without thermal activation. The MSTC is either used directly as a heat source for the heat pump or, more importantly, is used for the regeneration of the GCTES. According to the footprint of the building, the GCTES covers an area of 180 m², activated by a horizontal PE-piping with three parallel circuits of 100 m length each. As it is located underneath the building, it must be actively regenerated, unlike traditional ground collectors where solar radiation passively regenerates the ground around the collector during the summer season. The thermal capacity of the GCTES is determined by the covered ground area and the properties of the underground. As freezing the ground around the collector would damage the building the heat extraction from the storage is limited in terms of heat content and momentaneous heat flow. Consequently, it cannot serve as the only heat source for the heat pump throughout the heating season but must be supplemented by alternative ambient heat sources. During moderate ambient conditions, ambient air can be utilized as ambient heat source, allowing for efficient operation of the heat pump. Simultaneously, the GCTES can be regenerated during the heating season, resulting in a medium-term loading/unloading regime, instead of a purely seasonal cycling of the storage.

As a consequence of the increased annual heat output the economic efficiency of the GCTES is improved by means of the medium-term cycling with repeated regeneration during the heating season as compared to pure seasonal cycling. The system concept is depicted in Figure 1, showing the three heat sources for the heat pump and the regeneration of the GCTES by the MSTC.

The system is installed and investigated in a pilot plant. The hydraulic scheme of the plant is shown in Figure 2. The system provides heating for two building sections (“old” and “new”) via two separate heating circuits. The heat sources AAHX, MSTC, and GCTES are connected to the heat pump via a Zortström energy center [6]. Acting as a hydraulic switch it allows for different hydraulic configurations of the heat sources for the heat pump. Every heat source can be used alone or parallel or in series to one or two other heat sources. During air-sourced operation of the heat pump, the AAHX is coupled to the evaporator of the heat pump via the two bottom sections of the Zortström energy center. Simultaneously, heat gained by the MSTC can be transferred to the GCTES for regeneration via the two top sections of the Zortström energy center. Further information about the pilot plant and the analysis of the operating data can be found in [7, 8].

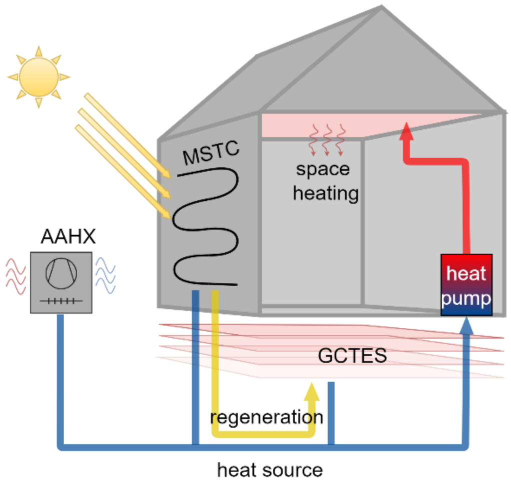

Figure 1. Schematic of the heat pump system with three heat sources.

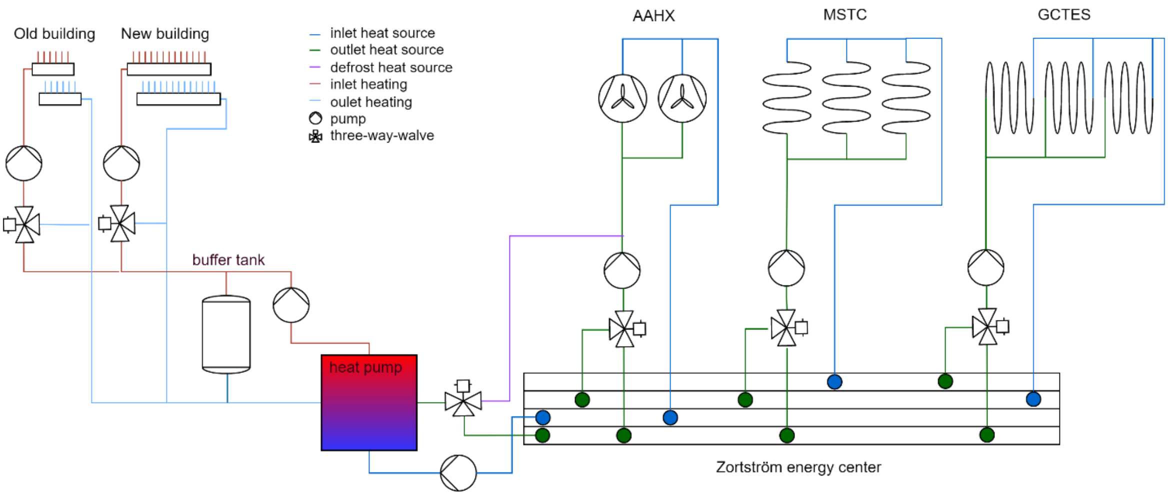

Figure 2. Hydraulic scheme of the heat pump system with three heat sources.

3. Modelling of the heat pump system

A theoretic model has been set up for analysis and optimization of the performance of the heat pump system with three heat sources, based on the software Engineering Equation Solver (EES). The heat load of the building and the thermal performance of the three heat sources were validated with reference to real-life data of the pilot plant. As a basis for the ambient weather conditions the test reference year "TRY" [9] for a location in the region of Nuremberg, Germany, is used.

In the following sections the models for the different system components are presented, which are then interlinked to represent the interaction of the system components within the heat pump heating system.

3.1. MSTC

The MSTC is formed by the outer shell of a prefabricated concrete sandwich wall. The wall structure is shown in Figure 3 where the outer concrete layer incorporates the heat carrier pipes for the extraction of the solar thermal heat gain. The insulation and inner concrete wall are shown without scale. On the surface of the MSTC radiation and heat transfer takes place, as shown in Figure 3.a. The solar yield $\dot{q}_{yield}$ of the MSTC results from a balance of the short-wave radiation E_{sw}, the long-wave radiation E_{lw}, and the convective heat flow $\dot{q}_c$, as defined in Eq. 1.

$$\dot{q}_{yield} = E_{sw} + E_{lw} + \dot{q}_c \tag{1}$$

The short-wave radiation E_{sw} is calculated by Eq. 2, where the absorption coefficient $\alpha_{c_{sw}}$ for short-wave radiation is 0.66 for gray concrete surfaces, according to [10]. The total shortwave radiation on the vertical absorber surface consists of the direct radiation $E_{sw,dir}$, the diffuse radiation $E_{sw,diff}$ and the radiation reflected from the ground $E_{sw,refl}$ on the inclined surface, see Eq. 2.

$$E_{sw} = \alpha_{c_{sw}} \cdot E_{g_{abs}} = \alpha_{c_{sw}} \cdot (E_{sw,dir} + E_{sw,diff} + E_{sw,refl}) \tag{2}$$

The exchange of long-wave radiation E_{lw} between two bodies is calculated in Eq. 3 and according to [11]. Here, the environment is formed by the sky and the ground, which are considered to be black bodies, with emission $E_{lw,sky}$, and $E_{lw,ground}$, while the absorber is a gray body with emissivity ε_{abs} and absorptivity α_{abs} equal to 0.95. σ is the Stefan-Boltzmann constant. T_{sky} is estimated according to [12] and [13], whereas the surface temperature of the surrounding earth T_{ground} is obtained from the model of the GCTES.

$$E_{lw} = \frac{1}{2} \cdot E_{lw,sky} + \frac{1}{2} \cdot E_{lw,ground} = -\sigma \cdot \varepsilon_{abs} \cdot \left(T_{abs}^4 - \frac{1}{2} \cdot T_{sky}^4 - \frac{1}{2} \cdot T_{ground}^4\right) \tag{3}$$

Depending on the ambient temperature T_a compared to the absorber temperature T_{abs}, the convective heat flow $\dot{q}_c$ (Eq. 4) is either a heat gain or heat loss. The effective heat transfer coefficient of convection α_{conv} results from a superposition of natural and forced convection due to buoyancy and wind, respectively. As given in [14] and [15], the exponent n=3 is used for super-positioning natural and forced convection.

$$\dot{q}_c = -\alpha_{conv} \cdot (T_{abs} - T_a) = -\sqrt[3]{\alpha_{c_{nat}}^3 + \alpha_{c_{forced}}^3} \cdot (T_{abs} - T_a) \tag{4}$$

From the surface of the MSTC the heat $\dot{q}_{yield}$ is conducted to the core of the concrete layer. Eq. 5 determines the energy balance for the central node with temperature T_{core} of the resistance model in Figure 3.b, see also [10,14]. Where $\dot{q}_{water}$ is the thermal power conducted to the collector pipes and exchanged to the heat transfer fluid for further distribution to the heat pump or GCTES. $\dot{q}_b$ or $\dot{q}_{room}$ is the heat conduction to or from the inside of the building. $\dot{q}_{concrete}$ is the heat that remains in the concrete and is stored for following time steps. It can also be negative, when the heat is extracted by the heat carrier or lost via the absorber surface.

$$\dot{q}_{yield} = \dot{q}_{water} + \dot{q}_{room} + \dot{q}_{concrete} \tag{5}$$

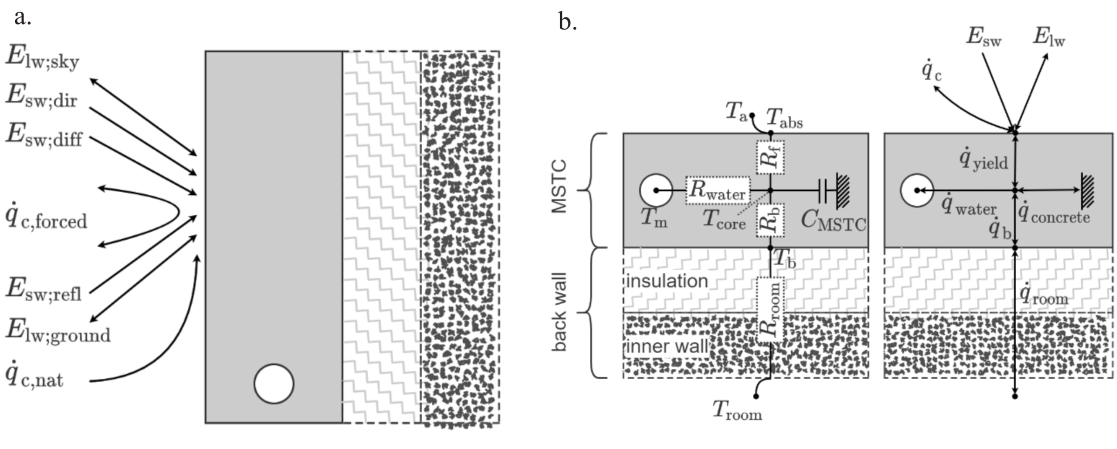

Figure 3. a. Heat and radiation exchange at the surface of the MSTC; b. resistance model of the MSTC.

3.2. GCTES

For modeling the behavior of the underground heat storage (GCTES), a finite volume approach is applied. The core volume underneath the building is divided into nine horizontal layers (layers 0...8) with increasing thickness. Below the bottom layer an isothermal situation with annually constant temperature of 11 °C is assumed. In the surrounding of the building, six cells with increasing length follow until undisturbed conditions are assumed forming the boundary condition in horizontal direction.

The collector tubes are positioned in the center of layer 0. A shape factor according to [16] in Eq. 6 and 7 is used for the conductive heat transfer from the heat carrier tubes to the planar surface of the underlying soil cell. The thermal power $\dot{Q}_{sf}$ is dependent on the conductivity of the ground λ, the shape factor S_l, the length of the pipe l and the temperature difference between the surface of the collector tube T_{tube} and the temperature of the first planar cell below the collector $T[0;0]$.

$$\dot{Q}_{sf} = \lambda \cdot S_l \cdot l \cdot (T_{tube} - T[0;0]) \tag{6}$$

$$S_l = \frac{2\pi}{\frac{\pi d}{\delta} + ln\frac{\delta}{\pi r}} \tag{7}$$

Inside the storage heat is distributed vertically to lower layers of the storage and horizontally to the surrounding earth. Due to the rectangular footprint of the building a three-dimensional problem is given. Nevertheless, in order to reduce the computational effort, a rotationally symmetric geometry has been selected, thus enabling a simplified two-dimensional geometric calculation. The core volume of the storage underneath the building is formed by a cylindric volume with identical outer surface area in contact to the surrounding soil as compared to the cubic volume of the real underground storage volume. To limit the computational effort, the dimensions of the cells grow stepwise by a factor of 1,435 in vertical and by 1.5 in horizontal direction. In ten meters depth the boundary layer is considered isothermal at 11 °C and in horizontal direction in a distance of 10,47 m the vertical temperature profile is assumed to be undisturbed, i.e. he ground temperature exhibits a characteristic oscillation that follows the annual cycle of weather conditions. Propagation of the heat flow is modelled by a forward explicit difference method. Attention is paid to the stability of the calculation by adhering to the Fourier number.

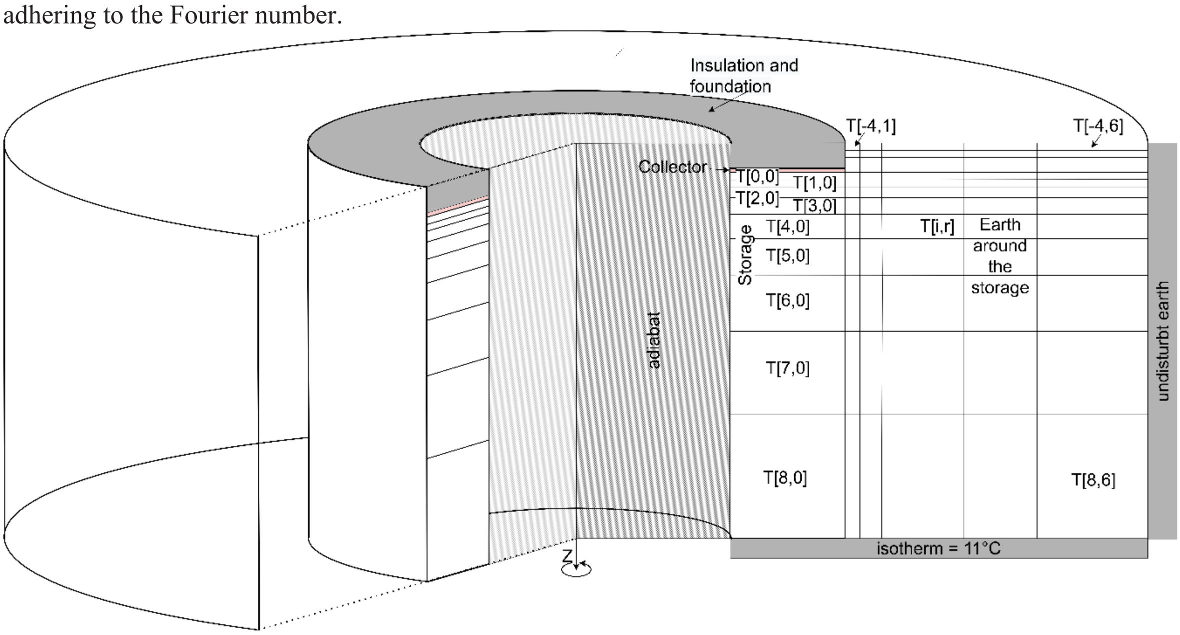

Figure 4. Cross-section the ground with the building top left, the GCTES underneath, surrounding earth and the boundaries at the bottom and the undisturbed earth on the right.

In addition to the heat flow induced by the ground collector heat exchanger circuit, the model incorporates the coupling of the surrounding earth with the momentaneous ambient weather situation. At the surface layer, with temperatures T[-4;1]… T[-4;7], exchange of radiation and convective heat transfer take place as shown in Figure 5, calculated according to [17]. The situation is similar to the radiative and convective mechanisms occurring at the surface of the vertical concrete wall. As the ground is horizontal, long-wave radiation is only exchanged with the sky, and superposition of natural and forced convection does not apply for the situation given. Instead, the maximum of the respective heat transfer coefficients is used to determine the convective heat exchange in Eq. 8 with surface temperature of the earth T_S and ambient temperature T_a.

$$\dot{q}_c = max\,(\alpha_{c_{forced}}; \alpha_{c_{nat}}) \cdot (T_S - T_a) \tag{8}$$

To accurately determine the temperature of surface layers up to one meter depth, the phase change of the contained moisture of the earth and the associated latent heat are considered.

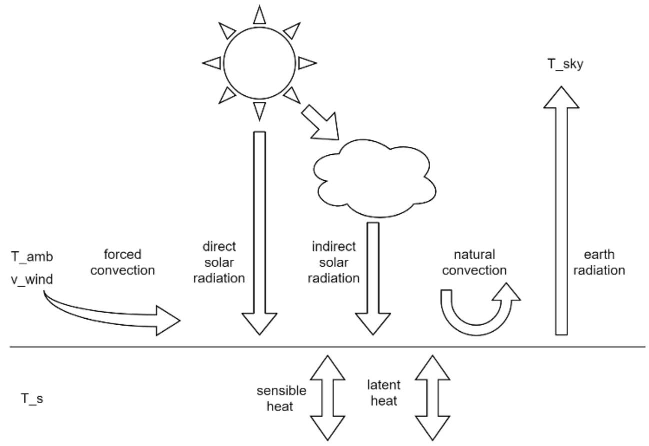

Figure 5. Exchange of heat and radiation at the surface of the earth around the GCTES.

3.3. AAHX

The AAHX represents a finned tube heat exchanger. Its thermal model has been based on the formulation for tube bundles with continuous fins, as given in [16].

The occurrence of frost in the AAHX during humid and cold ambient conditions is considered to make a significant contribution to the lower efficiency of air-source heat pumps in comparison to ground-source heat pumps. When a frost layer forms on the outer surface of the fins, the heat transfer in the AAHX decreases due to the increase of the thermal resistance and the reduced air flow rate, both induced by the blockage of the fins by the frost layer. In addition, a defrosting mode has to be activated repeatedly to remove the frost layer, resulting in additional energy consumption and a further decrease of the energetic efficiency.

In the system model, the additional electric demand for defrosting the AAHX is accounted for by a reduction of the COP, obtained from the heat pump model for operation without activation of the defrosting procedure. Referring to [18], a reduction of the COP from 11 % to 21 % occurs, depending on the operating conditions given by the temperature and humidity of the ambient air and the supply temperature of the heating system.

Considering the defrosting procedure to have the dominating influence on the efficiency of the heat pump, the decrease of the COP during continuous operation induced by the formation of frost is neglected in the system model. This conservative approach is chosen in order to avoid an overly optimistic judgement of the innovative heating system relative to a purely air-sourced heat pump.

3.4. Building

The building comprises a new building section with 180 m² and high insulation standard and an existing building section with 100 m² and lower insulation standard, both are heated by activated ceilings. The heating load of the building is determined using the envelope area method [19]. The heating circuit supply temperature is dependent on the ambient air temperature. According to its higher specific heat demand, the heating curve for the old building determines the temperature set point for the heat pump. At lowest ambient temperature, i.e. at the design point, a maximum supply temperature of 37 °C must be provided.

3.5. Heat pump

For the description of the operation of the heat pump under variable operating conditions a model based on key figures for the efficiency of the compressor, the selected refrigerant, and the heat exchange in evaporator and condenser of the heat pump is applied [20]. The model provides the COP of the heat pump, resulting from the outlet temperatures of the brine and the heating circuit at evaporator and condenser, and the heating load.

Starting from the temperatures of the heat carriers, the internal temperature levels of evaporation and condensation are determined by gradient model which describes the closest approach between refrigerant and external heat carrier: For the temperature difference between condensation and heating circuit fluid a closest approach of 1 K is assumed, considering the contribution of the superheated refrigerant entering the condenser.

The closest approach temperature at the evaporator between brine outlet and evaporation varies proportionately with the load, starting from 5 K in full load. This refers to latest advancements where the superheating of the refrigerant in the evaporator is accomplished by subcooling the refrigerant leaving the condenser [21].

A scroll compressor for the refrigerant R290 of suitable size was selected for the heat pump model. Its efficiency is described by compressor polynomials, as provided by the manufacturer according to DIN EN 12900 [22]. The efficiency of the compressor is obtained depending on the process-internal temperatures of evaporation and condensation, and the part load state of the heat pump. With the characteristics of the refrigerant, an efficiency value is employed, describing the loss in efficiency that is induced by the isenthalpic throttling process of the real heat pump cycle relative to the isentropic optimum.

3.6. System model – control strategy

In order to optimize the control strategy of the system, a simulation model has been developed that combines the previously described models into a single system model. To this end, four distinct control strategy setups have been developed and compared:

a) Heat source: AAHX | variable-speed heat pump
b) Heat sources: AAHX, MSTC, GCTES | single-speed heat pump
c) Heat sources: AAHX, MSTC, GCTES | variable-speed heat pump
d) Heat sources: AAHX, MSTC, GCTES | variable-speed heat pump with night setback (compressor speed reduction).

Case *a* describes a conventional air-source heat pump system, serving as reference. In cases *b*, *c*, and *d*, all three heat sources AAHX, MSTC, and GCTES are active, with different configurations of the heat pump. In order to enhance the contribution of the GCTES, a variable-speed heat pump is applied in cases *c* and *d*. In case *d*, a night setback is applied by reducing the load of the heat pump. This configuration represents the most complex control strategy, as illustrated in Figure 6.

In general, the control strategies for the cases *b*, *c*, and *d* have two fulfill two central tasks, i.e. the selection of the ambient heat source for heat input into the evaporator of the heat pump, and the regeneration of the GCTES by the solar heat gain of the MSTC. The upper section of Figure 6 deals with situations in which the building does not require any heating. Then, regeneration is activated when the following criteria (C1) are fulfilled: the temperature of the MSTC T_{MSTC} is two Kelvin (DR) higher than the temperature of the GCTES T_{GCTES}, enabling the heat transfer from the solar absorber to the thermal storage. And the absorber temperature T_{abs} is higher than the ambient air dewpoint T_{dew}, guaranteeing that no dew is formed on the surface of the MSTC. Else, regeneration is not possible and the system is on standby.

In the lower section of figure 6, the heat source for the heat pump is determined, while simultaneously regeneration of the GCTES is activated if possible. Thus, in a first step the possibility of recharging the GCTES is checked, guided by the same criteria C2 as in the situation without heating load (C1). If criteria C2 are fulfilled, regeneration of the GCTES is activated and the AAHX is utilized as ambient heat source.

If no regeneration is possible, a sequential routine is started for selection of the ambient heat source, giving the MSTC the highest priority over the GCTES and the AAHX. The criteria for the use of the MSTC are formulated in C3: The temperature of the MSTC must be higher than the temperature of the AAHX T_{AAHX}. And again, for esthetical reasons the MSTC must stay above the dewpoint. Subcriterion C3a determines that the MSTC acts as the sole ambient heat source, if its temperature is higher than the temperature of the underground heat storage GCTES. Otherwise, the MSTC and the GCTES can be used jointly in a serial configuration, where the brine is preheated by the MSTC before extracting heat from the GCTES. The criteria for this mode, formulated in Subcriterion C3b, result from the temperature gradients at both heat exchangers: The temperature of the GCTES has to qualify the GCTES as the best heat source, and the temperature of the MSTC is only 1.5 K (DT) below the GCTES.

For the GCTES to be used as the best heat source, different aspects have to be taken into account, as formulated in C4: The GCTES offers ambient heat at higher temperature level than the AAHX and the brine temperature passing through the GCTES stays above freezing (T_{Frost}) in order to avoid a damage of the building. Finally, the heat extraction from the GCTES must be controlled to retain sufficient heat content for colder weather periods. For this purpose, a temperature limit $T_{strategy}$ is incorporated in the control strategy. When the ambient air is above the temperature limit $T_{strategy}$ the AAHX provides ambient heat at sufficiently high temperature, enabling efficient operation of the heat pump. Even if the GCTES offers a higher temperature level, the heat content of the GCTES is withheld for colder winter days. Different set-values for the temperature limit $T_{strategy}$ have been analyzed in [8].

Subcriteria C4a and C4b are used to maximize the utilization of the GCTES: The temperature of the brine at the outlet of the GCTES ($T_{GCTES;out}$) may not drop below $T_{Frost;fluid}$ (0 °C) to avoid frost around the collector tubes. If this criterion is violated during regular operation of the heat pump, a night setback is activated by operating the heat pump with reduced speed of the compressor, resulting in a reduced heat extraction from the GCTES and a closer approach of the brine temperature to the frost limit. The activation of the night setback is restricted to nocturnal hours from 10 pm to 9 am.

If none of the other heat sources are chosen, the AAHX is used as heat source for the heat pump. This is the case, when the AAHX is the optimal heat source or when the other heat sources are not available and the AAHX serves as backup.

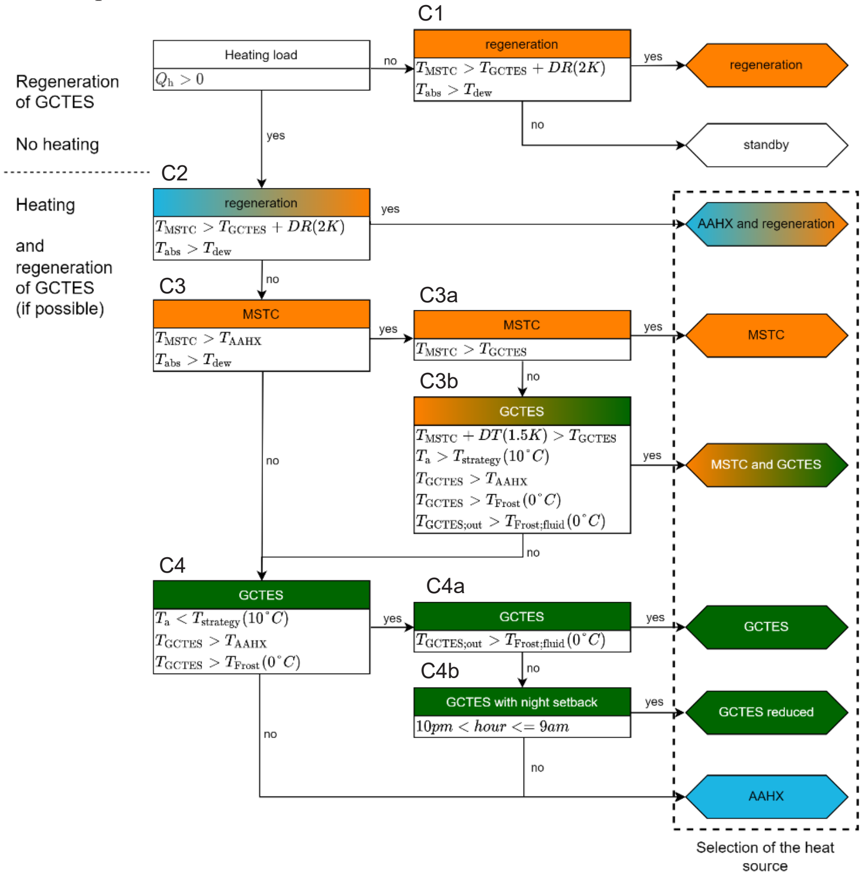

Figure 6. Flow chart for control strategy setup *d*.

4. Results and Discussion

The research goal for the different control strategy setups is to determine whether an increased heat extraction from the heat storage, trough discharging the storage to lower temperatures, results in a higher seasonal efficiency of the heat pump system. As the GCTES must be protected from frost, a reduction in the thermal power of the heat extraction allows for a closer temperature approach of the brine and the heat storage. The GCTES reaches lower temperatures, allowing an enhanced for contribution of the GCTES as ambient heat source for the heat pump. Therefore, the results for the system with all three heat sources and a single-speed heat pump (*b*) are compared to a configuration with a variable-speed heat pump (*c*), which operates with variable thermal power of heat extraction according to the heating load of the building. In control strategy setup *d,* a night setback is used in cold winter nights. The heat extraction is reduced below what is necessary to provide the heating load of the building. This allows for extended usage of the GCTES instead of the AAHX, which improves the COP. The deficit in heat supply to the building due to the night setback is compensated for over the course of the forthcoming day. As a comparison the system configurations *b*, *c*, and *d* comprising all three heat sources is contrasted with a system containing solely the AAHX as an ambient heat source (*a*).

The results for the annual temperature of the GCTES, show a decreased GCTES temperature level during the heating season for the cases with variable-speed heat pump (*c* and *d*) compared to the single-speed heat pump (*b*). The operation mode with night setback (*d*), allows for a further decrease in the GCTES temperature. Figure 7 (left) shows a comparison of the GCTES temperature in the top elemental cell $T[0;0]$. Figure 7 on the right shows the temperature of the GCTES in all nine layers below the collector for setup *d*. For the deeper ground layers, a stronger temporal delay of the heat extraction and regeneration in dependence on the distance to the collector in the top layer is identified, with the nineth cell being isotherm at 11 °C.

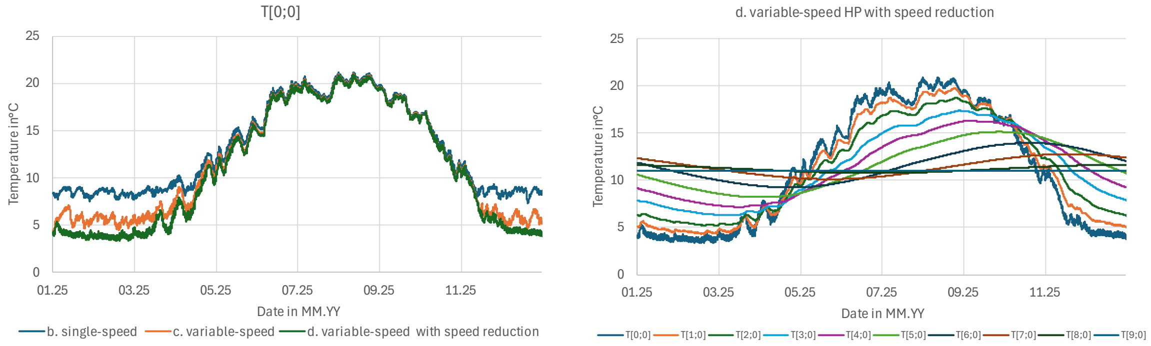

Figure 7. Comparison of the temperatures in the first cell T[0; 0] in setup *b*, *c* and *d* (left) and GCTES temperatures for control strategy setup *d* for elemental cells to 10 m depth (right).

The lower the minimum level of the GCTES temperature, the higher is the potential for overall heat extraction from the GCTES. This is due to the higher seasonal temperature oscillation between charged and discharged state of the storage, resulting in a higher heat content in the course of a seasonal storage cycle. In addition, a lower temperature level of the GCTES facilitates inter-seasonal regeneration by solar yields from the MSTC, and simultaneously supports the geothermal yield obtained by heat conduction from the surrounding earth. The inter-seasonal regeneration has been analyzed by the author in [8].

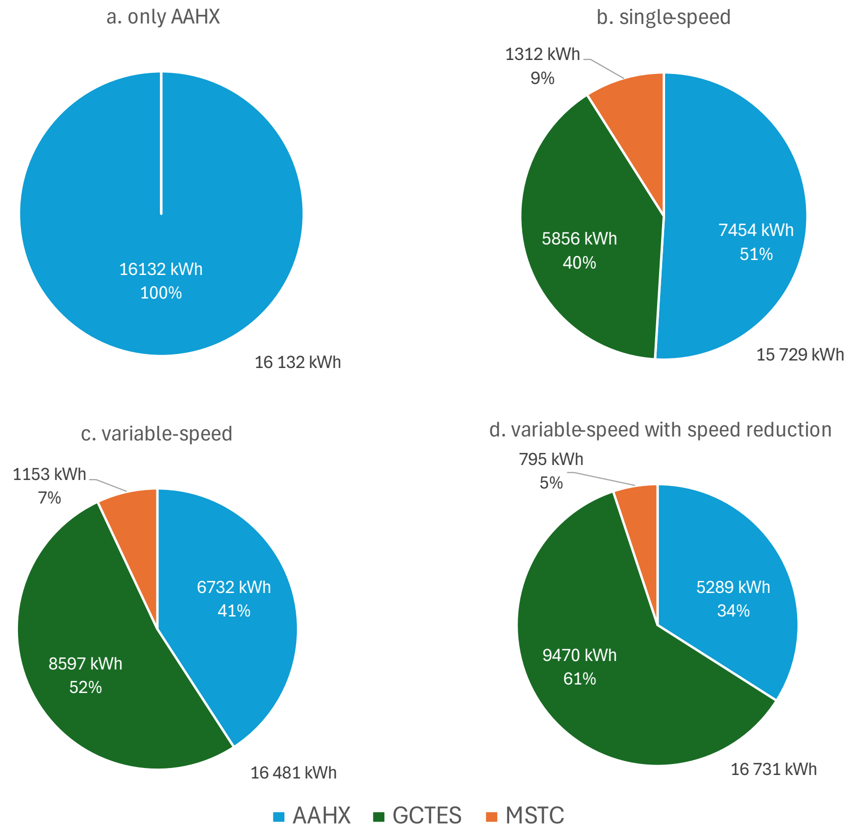

Figure 8. Heat provided by the heat sources for the heat pump in kWh and %.

Resulting from the different temperature profiles of the GCTES, the amount of heat extracted from the GCTES is increased by applying a variable-speed heat pump (*c*) and further by applying the night setback (*d*) relative to the reference setup *a* (pure air-source heat pump) and setup *b* (fixed-speed heat pump), as shown in Figure 8. The direct contribution of the MSTC as a heat source is comparatively low, relative to the other heat sources. This is due to the intention to use the MSTC mainly for the regeneration of the GCTES, which reduces the usage as a heat source. The lower the GCTES temperature, the more heat from the MSTC can be used for regeneration, and thus is not available as a heat source for the heat pump.

The higher the usage of the GCTES and MSTC the lower the heat provided by the AAHX as backup heat source. Depending on the time of usage of the AAHX and the corresponding ambient air temperatures, operation of the heat pump with low heat source temperatures and therefore low COPs can be reduced.

The control strategy in setup *d* is aiming to replace the AAHX as a heat source for the heat pump during cold winter nights. The difference during operation between setup *c* and *d* is shown in Figure 9. The heat source temperatures T_a and $T[0;0]$, the fluid temperatures $T_{AAHX;in}$, $T_{AAHX;out}$, $T_{GCTES;in}$ and $T_{GCTES;out}$ (bottom), the heating load of the building Q_h and reduced heating load Q_{hr} (middle) as well as the COP (top) are displayed. Apart from identical weather conditions, for both setups the GCTES temperature was set to the same starting conditions in order to enable a fair comparison.

In setup *c* the GCTES is unable to meet the heating load during the night-time hours, since the brine temperatures would be too low for a frost-safe operation. The AAHX is used as the backup heat source. As the ambient air temperatures are severely cold, especially in the second night, the COP drops during nighttime. In setup *d*, during the specified night hours, the GCTES is used as a heat source, but with a reduced heat extraction from the GCTES. Due to the higher temperature of the heat source, a higher COP than in setup *c* is attained. Following the nighttime period, the deficit of the heat supply is balanced by a higher load of the heat pump during the daytime, when ambient air temperatures are higher. During this balancing phase the COP is lower than in the scenario without night setback. As the GCTES is used more intensely in setup *d,* a larger amount of heat is extracted, resulting in a stronger decrease of the temperature of the GCTES than in setup *c*.

As a conclusion regarding the shown operating period, it is found that in setup *d* the GCTES is only used during the night setback phase. In contrast, in setup *c*. the GCTES can't be used during the night to avoid frost. It is then used during the day, when elevated ambient air temperatures would also allow for efficient operation of the heat pump in air-sourced mode. Finally, when the entire period of severely cold winter days shown in Figure 9 is evaluated, an increase of the COP from 2.73 for setup *c* to 3.47 for setup *d* is found.

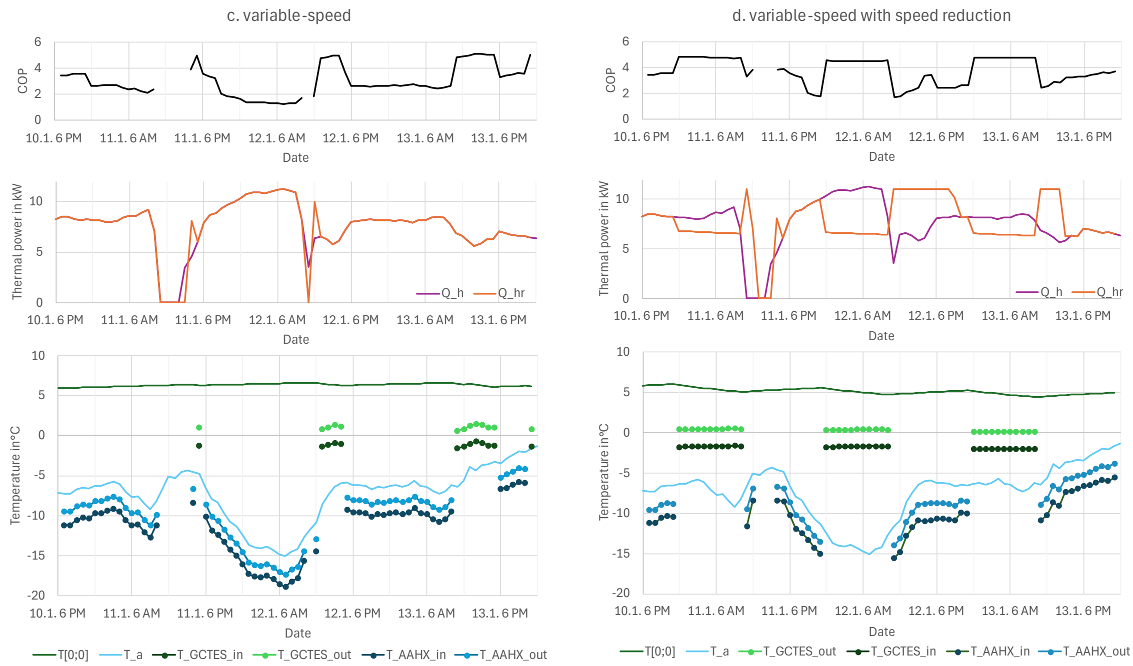

Figure 9. COP (top), heating load and reduced heating load (middle), and heat source and corresponding fluid temperatures (bottom) for control strategy setup *c* (left) and *d* (right).

As the control setups with a variable-speed heat pump allow for an increased annual heat extraction from the GCTES, the timing of the usage has a strong influence on the improvement of the system. In Figure 10 the monthly sums of the heat provided by the respective heat sources is shown for the four control strategy setups. Comparing the setups with all three heat sources, the amount of heat from the GCTES rises from setup *b* to *d* during the cold winter month December till March. Also, more inter-seasonal regeneration of the GCTES by the MSTC (MSTC regeneration) takes place, because of the lower GCTES temperatures.

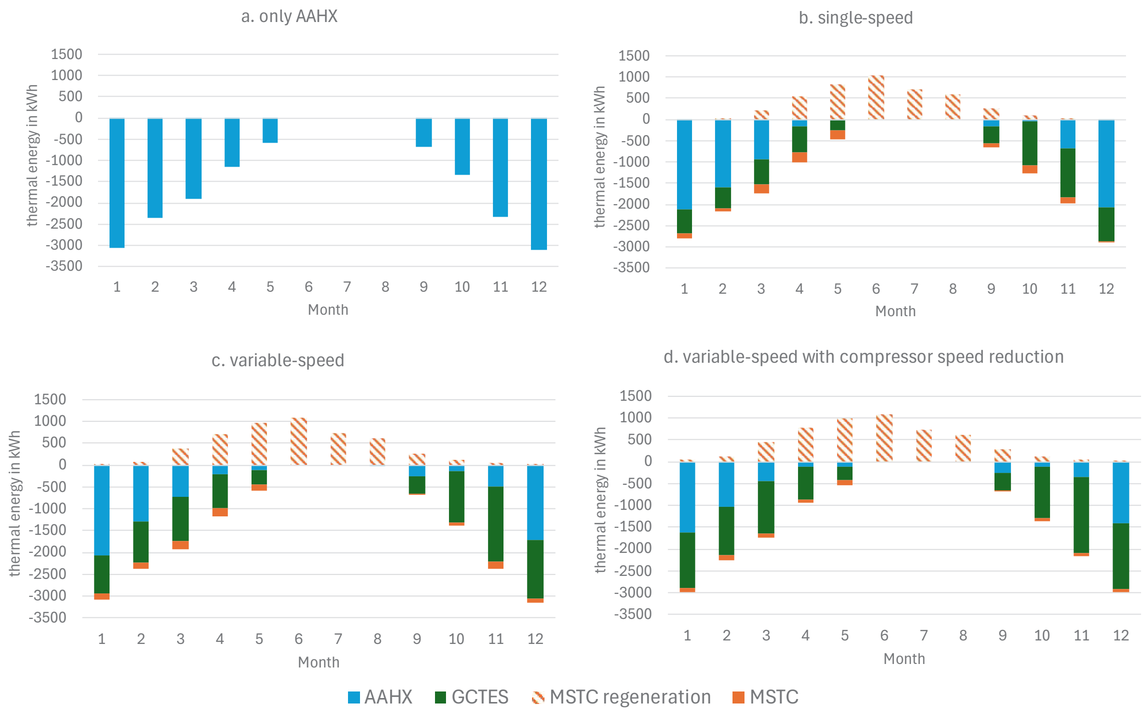

Figure 10. Thermal energy for all heat sources and monthly average COP.

The difference of the temperature levels of the ambient heat sources lead to diverging COP values for the four control setups. The monthly average COP of the four control strategy setups are compared in Figure 11. Control strategy setup *b* shows the lowest monthly average COP values, where the high compressor speed of a single-speed heat pump results in higher thermal power for the heat extraction and therefore lower evaporation temperatures. Even then, the high GCTES temperatures in September and October allow for a higher COP compared to setup *a* with only the AAHX as a heat source. Setup *c* and *d* have both higher monthly average COP values than in setup *a*. When investigating the effect of the night setback, a higher COP is found for setup *d* during cold winter month December till March, due to higher and more efficient utilization of the GCTES. On the other hand, a lower COP is achieved in spring, when the GCTES is still colder in setup *d* than in setup *c*. Overall, the seasonal coefficient of performance “SCOP” is lowest for setup *b* equal to 3.99, while the SCOP for reference configuration (setup *a*) is 4.29. Best efficiencies are achieved by setup *c* with SCOP 4.63 and setup *d* with SCOP equal to 4.91, proving an increased SCOP for higher usage of the GCTES.

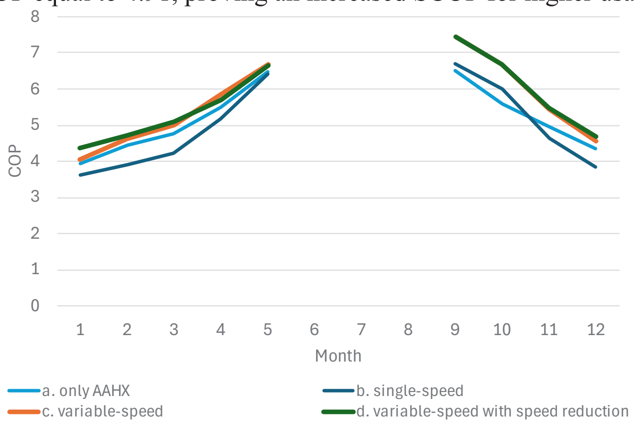

Figure 11. Monthly average COP for the four control strategy setups.

5. Conclusions

In this paper an air-source heat pump system supported by two additional ambient heat sources has been investigated. The effect of different modes of operation has been assessed to optimize the contribution of a ground collector thermal energy storage (GCTES) regenerated by a massive solar thermal collector (MSTC). It was found that, a variable-speed heat pump allows for lower GCTES temperatures and higher heat extraction from the GCTES. Further, the introduction of a night setback by operating the heat pump with reduced compressor speed allows for extended use of the GCTES during cold winter nights and thus avoids less efficient air-sourced operation of the heat pump. Based on these improvements, the heat extraction from the GCTES is increased, supported by inter-seasonal solar and geothermal regeneration, and the entire system reaches an improved seasonal performance compared to a purely air-based heat pump system.

Acknowledgements

The research project is funded by the German Federal Ministry for Economic Affairs and Climate Action under grant number 03EN1064A.

The support by Syspro-Gruppe Betonbauteile e. V. and MEIER Betonwerke GmbH is gratefully acknowledged.

References

[1] Günther D, Wapler J, Langner R, Helmling S, Miara M, Fischer D, Zimmermann D, Wolf T, Wille-Hausmann B. WPsmart im Bestand. Freiburg; 2020,

[2] Bundesverband Wärmepumpe e.V., https://www.waermepumpe.de/presse/zahlen-daten/, last accessed 2025/10/10.

[3] D'Antoni M, Saro O. "Massive Solar-Thermal Collectors: A critical literature review," *Renewable and Sustainable Energy Reviews*, vol. 16, no. 6, pp. 3666–3679; 2012

[4] Aquilanti A, Peralta I, Koenders EAB, Nicola GDi. "A Brief Review of the Latest Advancements of Massive Solar Thermal Collectors," *Energies*, vol. 16, no. 16, p. 5953; 2023

[5] Tanzer B, Schweigler C. "Façade-integrated Massive Solar-thermal Collectors Combined with Long-term Underground Heat Storage for Space Heating," *Energy Procedia*, vol. 91, pp. 505–516; 2016

[6] Zortea, https://www.zortea.at/en/zortstroem-technology/, last accessed 2024/01/14.

[7] Lauffer A., Schweigler C., 2023 Wärmepumpenheizsysteme mit mehreren Wärmequellen, *Deutsche Kälte-Klima-Tagung 2023*, Hannover

[8] Lauffer A., Schweigler C., Niemann T., 2025 "Control strategy for a heat pump system with a solar regenerated medium-term ground collector thermal energy storage and ambient air as heat sources"; *Clima2025 Conference*, Milan

[9] Climate consulting module, https://kunden.dwd.de/obt/, last accessed 2022/09/22.

[10] Tanzer B., 2019. Solarthermische Massivabsorber und Langzeitwärmespeicher.

[11] Baehr HD, Stephan K. Wärme- und Stoffübertragung; *Springer Berlin Heidelberg* 2019

[12] O'Hegarty R., Kinnane O., McCormack S. J., 2017. Concrete solar collectors for façade integration: An experimental and numerical investigation. Elsevier BV Applied Energy

[13] Martin M., Berdahl P., 1984. Characteristics of infrared sky radiation in the United States. Elsevier BV Solar Energy

[14] Tanzer B., Schweigler C., Eberherr H., Laumer R., 2017. Abschlussbericht des Forschungsvorhabens: Solarwärmesystem für die Beheizung von Industriehallen mit Massivabsorber und Saisonwärmespeicher

[15] Churchill S. W., 1977. A comprehensive correlating equation for laminar, assisting, forced and free convection. Wiley

[16] Verein Deutscher Ingenieure, Gesellschaft Verfahrenstechnik und Chemieingenieurwesen, 2013. VDI-Wärmeatlas.

[17] Jaszczur M., Polepszyc I., Biernacka B., Sapińska-Śliwa A., "A numerical model for ground temperature determination", *Journal of Physics: Conference Series*, vol. 745, p. 32007; 2016

[18] Kropas T., Streckienė G., Bielskus J., "Experimental Investigation of Frost Formation Influence on an Air Source Heat Pump Evaporator", *Energies 14(18), 5737;* 2021

[19] DIN EN 12831-1; Energetische Bewertung von Gebäuden –Verfahren zur Berechnung der Norm-Heizlast – Teil 1: Raumheizlast, Modul M3-3; 2017

[20] Bentz J., Schweigler C., Klüglich J., Roggenkamp T., Dynamische Optimierung von Kälteversorgungssystemen. Final report: ENOS - Dynamische Optimierung von Kälteversorgungssystemen. Grant no. BMWK-FKZ 03ETW009 A/B; 2024

[21] Ziegler F.J., „Hohe SCOP-Werte und 3K- Wasser-Wärmepumpen", *HK-Gebäudetechnik 5-25*, pp. 52-55

[22] DIN EN 12900; Refrigerant compressors – Rating conditions, tolerances and presentation of manufacturer's performance data; 2013